Available online at www.sciencedirect.com
ScienceDirect
Journal of the European Ceramic Society 29 (2009) 1613–1624
www.elsevier.com/locate/jeurceramsoc

# Effects of $Y_2O_3$ additives and powder purity on the densification and grain boundary composition of $Al_2O_3$/SiC nanocomposites

I.P. Shapiro *, R.I. Todd, J.M. Titchmarsh, S.G. Roberts

*University of Oxford, Department of Materials, Parks Road, Oxford OX1 3PH, UK*

Received 16 May 2008; received in revised form 2 September 2008; accepted 12 September 2008
Available online 5 November 2008

**Abstract**

Sub-micron sized SiC additions can be used to increase the wear resistance and change the fracture mode of $Al_2O_3$. However, these additions also restrict sintering.

$Al_2O_3$ and $Al_2O_3$–5%SiC 'nanocomposites' were prepared from alumina powders of high purity and of commercial-purity, with or without the addition of $Y_2O_3$. The effects of these compositional variables on sintering rate, final density and grain boundary composition were investigated. A direct comparison with $Al_2O_3$–$SiO_2$ composites was also made, as it has been proposed that SiC partially oxidises during processing of $Al_2O_3$–SiC nanocomposites.

The addition of 5 vol.% SiC to $Al_2O_3$ hindered densification, as did addition of 0.15 wt.% $Y_2O_3$ or 0.1 wt.% $SiO_2$. In contrast, the addition of 0.15 wt.% $Y_2O_3$ to $Al_2O_3$–5% SiC nanocomposites improved densification.

The composition of $Al_2O_3$–$Al_2O_3$ grain boundaries in these materials was studied using STEM and EDX microanalysis. The addition of SiC and $SiO_2$ caused segregation of Si, and $Y_2O_3$ addition caused segregation of Y. The segregation of each element was equivalent to <10% of a monolayer at the grain boundary. However, if SiC and $Y_2O_3$ were simultaneously added the segregation increased to 40% of a monolayer. The enhanced segregation was attributed to increased oxidation of SiC in the presence of $Y_2O_3$ allowing formation of a $SiO_2$–$Al_2O_3$–$Y_2O_3$ eutectic phase or a segregated layer which may explain the improvement in sintering rate when $Y_2O_3$ was added to nanocomposites.


*Keywords:* Sintering; Grain boundaries; Nanocomposites; $Al_2O_3$; SiC

## 1. Introduction

### 1.1. $Al_2O_3$–SiC nanocomposites

Early researchers found a large (186%) increase in strength when sub-micron SiC particles were added to $Al_2O_3$ to form 'nanocomposites' (in most cases more correctly termed microcomposites).[1] More recent research[2–6] has found that for highly polished specimens, the strength increase, if any, of the nanocomposites over $Al_2O_3$ is more modest (0–64%). All studies, though, have found that there is a distinct change from intergranular fracture in $Al_2O_3$ to transgranular fracture in nanocomposites, regardless of the presence or magnitude of any strength increase.[1,2,4,7]

Early research suggested that the strength increase was accompanied by toughening of the materials,[1,2] although the consensus is now that there is no such toughening.[5,6] Hence, the various mechanisms that have been proposed for strength increases due to the inclusion of SiC in the nanocomposite which imply an increase in toughness are unlikely to be valid.

In the absence of real toughness increases, there remain essentially two mechanisms for an increase in strength of the nanocomposites compared with $Al_2O_3$:

1. Reduction in the size of the critical fracture-generating flaws. Perez-Rigueiro et al.[6] noted that "the mechanical properties of the nanocomposites are more sensitive to the processing details than to the size and volume fraction of the SiC particles". One possible reason for this is that, during milling of the powders, the SiC particles could break up agglomerates that lead to strength-reducing flaws during sintering.[5] However, in that case one might also expect other hard particles to

* Corresponding author at: Materials Science Centre, University of Manchester, Grosvenor Street, Manchester, M1 7HS, UK. Tel.: +44 161 306 3552.
*E-mail address:* ian.shapiro@manchester.ac.uk (I.P. Shapiro).

0955-2219/$ – see front matter © 2008 Elsevier Ltd. All rights reserved.
doi:10.1016/j.jeurceramsoc.2008.09.021

improve strength, which is not found to be the case for TiN particles added to $Al_2O_3$.[8] Sample surface preparation may also influence flaw sizes: nanocomposites have been found to have smaller surface flaws for a given surface finish than $Al_2O_3$ polished using the same sequence of abrasives;[9] such differences probably account for some part of the strength enhancements found. Flaw sizes may also be reduced by via crack healing during annealing at 1200–1300 °C.[1,10]

2. Reduction in the stress near-surface flaws are exposed to. $Al_2O_3$–SiC nanocomposites are found to have higher levels of compressive near-surface residual stresses than $Al_2O_3$ ground and polished using the same sequence of abrasives.[11–13] This may be because less of the plastically deformed material responsible for the compressive stresses is removed by grain pullout[14] and may also be related to differences in near-surface deformation modes between the materials: predominantly twinning in $Al_2O_3$, predominantly dislocation generation and motion in the $Al_2O_3$–SiC nanocomposites.[15]

A related factor is that $Al_2O_3$–SiC nanocomposites are harder to sinter to full density than $Al_2O_3$ as the SiC particles retard densification and grain growth (Section 1.3). Hence, the nanocomposites tend to have significantly finer grain sizes when fully dense than $Al_2O_3$.[9,16,17] Genuine improvements in properties can then be achieved simply by grain-refinement.

The wear behaviour of the nanocomposites is different from that of $Al_2O_3$, even for materials of the same grain size.[3,8] The propensity for grain pullout via grain boundary fracture in $Al_2O_3$ is substantially reduced in the nanocomposites (similar to the change on fracture paths noted above), leading to a reduction in wear rate under severe wear conditions.[3,14,18]

Descriptions and explanations of the changes in properties between $Al_2O_3$ and nanocomposites have focussed on the particles, especially the strengths of their interfaces with $Al_2O_3$[19–21] or residual stresses around them.[22,23] However, it is possible that the grain boundaries themselves are changed in either chemistry or structure by the presence of the SiC or by any sintering aid added, and that this might affect mechanical properties.

Dillon and Harmer have recently introduced the idea of 'complexion' to describe the nature of grain boundaries in doped $Al_2O_3$.[24,25] They categorise boundaries in terms of their mobility which coincides with distinct classes of grain boundary structures termed 'complexions'. A clean boundary is classed as complexion II; one with sub-monolayer dopant absorption but low mobility as I; and classes III–VI relate to boundaries with increasing thickness, segregation and mobility. While these categories were developed through the study of abnormal grain growth the distinct structures identified may also influence grain boundary diffusion in the densification process and the toughness of the boundaries.

### 1.2. Previous work on nanocomposite grain boundaries

Schmid et al.[26] found that $Al_2O_3$–SiC nanocomposites have Si segregation and a 0.9-nm thick glassy layer at the grain boundaries. Deng et al.[27] also found Si segregation in nanocomposites, and also segregation of $Y^{3+}$, $Nd^{3+}$ or $La^{3+}$ when 0.18 wt.% of these elements were added. However, they did not find a glassy grain boundary phase in any of their materials. Unfortunately neither of these studies made a comparison with similarly processed $Al_2O_3$ without the SiC addition. (Wu also found Si segregation in nanocomposites which increased after annealing).[10]

Interestingly, improvements in wear properties of nanocomposites over those of alumina have also been found when studying materials made with impure "easy sintering" alumina (Sumitomo AES 11c) which contains $SiO_2$ (0.04%), $Na_2O$ (0.03%) and MgO (0.04%).[9] This indicates that there is a change in properties when SiC is added even when compared to an alumina which would already be expected to have significant grain boundary segregation.

### 1.3. Processing of nanocomposites

The improved wear resistance and improved surface finish of nanocomposites may find a practical application. However, a significant barrier to industrial application of nanocomposites is their reduced sinterability compared to $Al_2O_3$. For example Stearns et al.[28] found that the addition of 0.15 μm SiC to $Al_2O_3$ caused a reduction in density from greater than 99% to 87% when sintered at 1400 °C. They found that sintering at 1700 °C was necessary to produce a 99% dense nanocomposite. Other studies have used hot pressing to produce fully dense nanocomposites.[1,4]

Stearns et al. made two suggestions as to how SiC particles inhibit densification.[28] They suggest that strong directional bonding of SiC means that diffusion along the $Al_2O_3$–SiC interface and removal of material from the $Al_2O_3$–SiC interface, both of which are necessary for densification, are slow.

Such high sintering temperatures or the necessity for hot pressing would hinder the materials' being adopted for industrial applications. To overcome this problem there has been several studies into possible sintering aids.

### 1.4. Sintering aids

Using less pure $Al_2O_3$ powder is partially effective at producing higher densities, however, sintering aid additions provide a greater effect.[16,29] MgO and $Y_2O_3$ have been investigated as sintering aids for $Al_2O_3$/SiC nanocomposites both individually and together.[30–33] Pillai et al.[32] found the most dramatic effect was with 1 wt.% $Y_2O_3$, increasing the density of a 5-vol.% SiC nanocomposite from 92% to 99% at only 1550 °C. Jeong et al.[31] attributed the beneficial effect of $Y_2O_3$ on sintering of nanocomposites to the formation of an $Al_2O_3$–$Y_2O_3$ glassy phase (lowest binary eutectic temperature ~1786 °C),[34] however, Pillai et al.[32] attribute the effect to the formation of an $Al_2O_3$–$Y_2O_3$–$SiO_2$ liquid phase during sintering (lowest ternary eutectic temperature ~1371 °C).[35] Pillai et al. based this conclusion on the presence of a glassy grain boundary phase ~1.5 nm thick containing a high atomic number element. Using the 'complexions' model this could be considered a type V boundary with high mobility.[25]

The study reported here investigates further the effects of $Y_2O_3$ on the sintering behaviour of $Al_2O_3$–SiC nanocomposites, in particular the effects of the additives on grain boundary chemistry. The effects were studied in two types of material: those made with pure starting powders with a processing route designed to exclude ingress of any impurities, and those made using commercial-grade easy-sintering alumina powder with a "standard" processing route.

## 2. Experimental methods

### 2.1. Processing procedure

Appropriate quantities of SiC (>97.4% pure, UF25, H.C. Stark, Germany), $SiO_2$ (99.8% pure, Aldrich, UK), $Y(NO_3)_3{\cdot}6H_2O$ (99.9% pure, BDH, UK; which decomposes to $Y_2O_3$ on heating) and $Al_2O_3$ were mixed as aqueous slurries and milled for 3 h. To help dispersion, 0.1 g of Dispex A40 (Ciba, Switzerland) was added and, to help green body formation, 4 wt.% polyethylene glycol (PEG) was added. 'Pure' processed materials were made using 99.99% pure $Al_2O_3$ (AKP50, Sumitomo, Japan) using a ball mill and $Al_2O_3$ media and 'standard' processed materials were made with 99.8% pure $Al_2O_3$ (AES11C, Sumitomo, Japan) using an attrition mill and $ZrO_2$ media. Powders were subsequently freeze-dried and uniaxially pressed at 137 MPa. Samples were sintered in a flowing $N_2$ atmosphere with a flow rate of 300 $cm^3$/min (Lenton High Temperature Furnace, UK). The furnace was heated at 3 °C/min and held at the sintering temperature for 120 min before cooling at the same rate.

### 2.2. Density measurement

The density of sintered samples was measured using a technique based on Archimedes' principle. The sample mass was measured dry, after boiling in water to absorb water into open porosity, and whilst submerged. The measurement accuracy was estimated as 0.3% of theoretical density which was calculated by assuming all the additions were present as the pure phases α-$Al_2O_3$, α-SiC, $Y_2O_3$ and $SiO_2$ in the same proportions as added.

### 2.3. Dilatometry

Green compacts (10.7 mm diameter, ~3.3 mm height) were sintered in a dilatometer (L75 V, Linseis, Germany). The heating rate (3 °C/min), hold time (120 min) and atmosphere (300 $cm^3$/min of $N_2$) were kept the same as previously; however, maximum temperature was restricted to 1550 °C by the dilatometer furnace.

The linear contraction was measured as the samples sintered. The contraction was considered to be isotropic which allowed the density at each temperature to be calculated from the green density and linear contraction. The green density was calculated from the mass and dimensions to an estimated accuracy of ±0.14 g/$cm^3$. The sintered mass rather than green mass of the sample was used to calculate green density so as to negate the loss in mass due to burning out of the PEG binder which would otherwise misleadingly imply a decrease in density.

### 2.4. Microstructural analysis and grain size measurement

Thermal etching was used to reveal the grain boundaries on polished surfaces by heating in a vacuum furnace (Lenton, $<10^{-8}$ mbar, 5 °C/min heating/cooling rate) to 1475 °C for 30 min. Field-emission SEM images (5–20 keV, 10–15 mm working distance, JEOL 840F, Japan) taken at 4k× and 7k× magnification were used to measure grain size using the linear intercept technique.[36] At least 175 intercepts were used for each micrograph. The grain size was estimated by dividing the mean number of intercepts by the line length on the sample and then multiplying by a correction factor, 1.56.[37]

### 2.5. TEM sample preparation

The sintered pellets were sliced along two parallel chords to form rectangular sections. The large faces of these sections were polished using 25 μm and then 6 μm diamond on both sides until their thickness was 100–200 μm. An ultrasonic drill (Gatan, USA) fitted with a hollow cylindrical tool was used to produce disks of 3 mm diameter from the polished rectangles. These disks were dimple-ground on both sides (Model 656, Gatan, USA).

The sample was thinned to electron transparency using a broad Ar ion beam in a Precision Ion Polishing System (PIPS, Model 691, Gatan, USA). Thinning took between 40 min and 120 min. Samples were carbon-coated (E306, Edwards, UK) to prevent charging in the TEM.

A conventional TEM (CM20, Philips, The Netherlands) was used at 200 keV to obtain bright-field images of each of the materials. Bright-field images of some particles were also captured in a dedicated cold field-emission scanning-TEM (STEM, HB501, Vacuum Generators, UK) operated at 100 keV.

### 2.6. Energy-dispersive X-ray microanalysis (EDX)

Energy-dispersive X-ray microanalysis (EDX) was performed on particles found, by: TEM (as above) with a thin-window detector (Link Pentafet 6767, Oxford Instruments, UK); STEM (as above) with a windowless detector (Link Pentafet 6969, Oxford Instruments, UK), using a focussed probe. Both detectors had a resolution of 136 eV at 5.9 keV. The X-ray spectra were quantified using INCA software (Oxford Instruments, UK).

Grain boundary composition was examined by STEM as follows. A well-defined, particle-free grain boundary was selected and tilted to make the boundary appear as narrow as possible and the image then focused. This ensured that the plane of the boundary was parallel to the beam direction, minimising the projected width of the boundary and hence maximising the X-ray signal from any segregated elements. Spectra were taken at positions 2.5 nm, 5 nm, 7.5 nm, 10 nm and 20 nm perpendicularly away from the boundary and on the boundary. At least one spectrum was captured at each location with at least 60 s 'live-time'.

For quantitative analysis, segregation was assumed to be a monolayer along the grain boundaries with width 0.2766 nm, the average inter-cation distance in $Al_2O_3$. The low segregation values obtained in this work suggest that monolayer segregation is likely to be a reasonable assumption and certainly provides a quantitative means to compare segregation between different boundaries. Segregation was calculated using a computer programme developed by Vatter and Titchmarsh.[38] A Gaussian distribution was fitted to the experimental data by a 'maximum likelihood' method in which the central location on the abscissa, height and standard deviation of the distribution were iteratively changed. Each measured point included an estimated uncertainty reported by the INCA software, which was considered to form a probability distribution for the composition at that point. For a particular fitted Gaussian distribution the probability of that fit at each measured point was multiplied by the probability of all the other points. The minimum value of this product was determined by iterative variation of all possible Gaussian parameters (position, height and width) to determine the most probable fit. By considering the error value at each datum the fitting was weighted towards more certain points where the probability distribution around the real value is smaller.

The accuracy of the quantified monolayer segregations was dependent on the uncertainties in composition at each point. The software[38] estimated the accuracy of fit from the distribution of the product of the probabilities of the measured values for fitted profiles with segregation levels around that of the most probable fit. This was reported by the software as one standard error, giving the 68% confidence range. A less certain fit will have a greater range of equally suitable fitted Gaussians, hence a larger standard error.

The minimum detectability of grain boundary segregation was estimated by considering the smallest definitively identifiable peak for a given background level. The count rate varied between samples depending on microscope conditions and sample thickness resulting in background counts in a window around the Si Kα[1,2] peak between 19 and 420 counts. If the smallest definitively identifiable peak is defined as four times the square root of this background the resulting minimum detectable Si concentration is between 0.14 wt.% and 0.26 wt.%, equivalent to a grain boundary segregation between 1.3% and 2.4% of a monolayer.

Theoretically calculated Cliff-Lorimer factors (k factors) are used by the Inca software to avoid the need for standards. The factors do not correct for absorption or fluorescence of X-rays; however, the absorption correction factor has been shown to be negligible even with a relatively thick (<200 nm), predominantly $Al_2O_3$, sample (for example, <1.09 for Si Kα compared to Al Kα, the most strongly absorbing combination). The fluorescence correction factor is also assumed to be negligible. The spatial resolution is estimated to be around 4 nm in a 100 nm thick $Al_2O_3$ sample for the STEM at 100 keV, which is consistent with the width of the composition profile of grain boundaries (Fig. 8).

The quantification method should not be affected by grain boundary alignment, skew, and probe size/focus as these factors will cause an increase in the width of the profile and a reduction of peak intensity, while the area used for quantification remains constant within experimental uncertainty.[39] However, the quantification method requires that the sample thickness is constant across the boundary. X-ray count rate was observed for probe positions across some boundaries and there was no variation which would have indicated a change in thickness.

Focus and specimen drift will also alter the segregate signal and make the grain boundary profile inaccurate. After each spectrum was acquired the image was checked for drift and if there was a noticeable drift out of focus or a specimen drift of greater than 2.5 nm the spectrum was discarded and a new analysis made.

## 3. Results

### 3.1. Sintering

The densities of the 'pure processed' materials are shown in Fig. 1 for various sintering temperatures. The $Al_2O_3$ material and the material with only 0.15 wt.% $Y_2O_3$ added both achieved nearly full density when sintered at 1550 °C although some porosity remained after sintering at 1650 °C. The porosity which remained at 1650 °C was attributed to abnormal grain growth causing trapped intragranular porosity. When 0.1 wt.% $SiO_2$ (with and without $Y_2O_3$) was added, density was decreased compared to $Al_2O_3$, which was also attributed to abnormal grain growth. When 5 vol.% SiC was added, density was further decreased, although less so when 0.15 wt.% $Y_2O_3$ was also added.

The sintered density of the 'standard processing' materials, also shown in Fig. 1, showed a similar trend. The $Al_2O_3$ materials and the material with only 0.15 wt.% $Y_2O_3$ added both achieved close to full density when sintered at 1550 °C (99.8% and 100.1%, respectively). The density also decreased when SiC was added, for example the 'standard processing' material with only SiC added achieved only 96.2% density and that with both SiC and $Y_2O_3$ added achieved 97.2% density when sintered at 1600 °C.

If the mass of binder was discounted, all samples used for dilatometry had green densities between 56.5% and 57.3% of theoretical density.

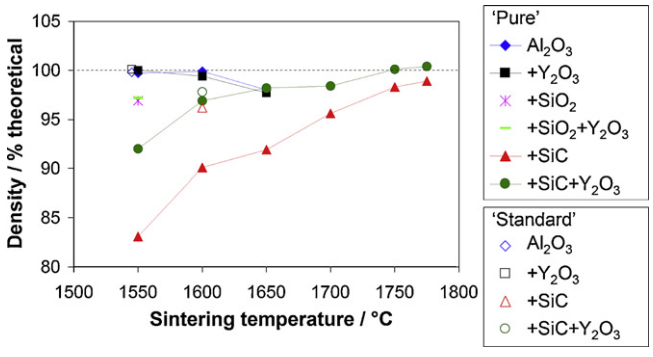


Fig. 1. Final density of 'pure' materials as a function of sintering temperature. The reduction in density when SiC is added is shown as is the beneficial effect of $Y_2O_3$ on density.

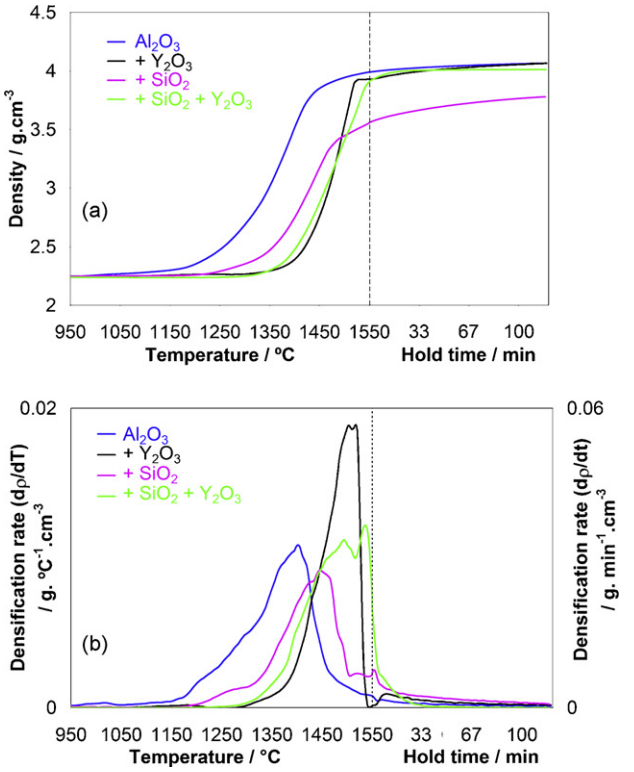


Fig. 2. Density during heating to 1550 °C and hold period (a) and differential showing rate of densification (b) for $Al_2O_3$ with and without $Y_2O_3$ and/or $SiO_2$ additions.

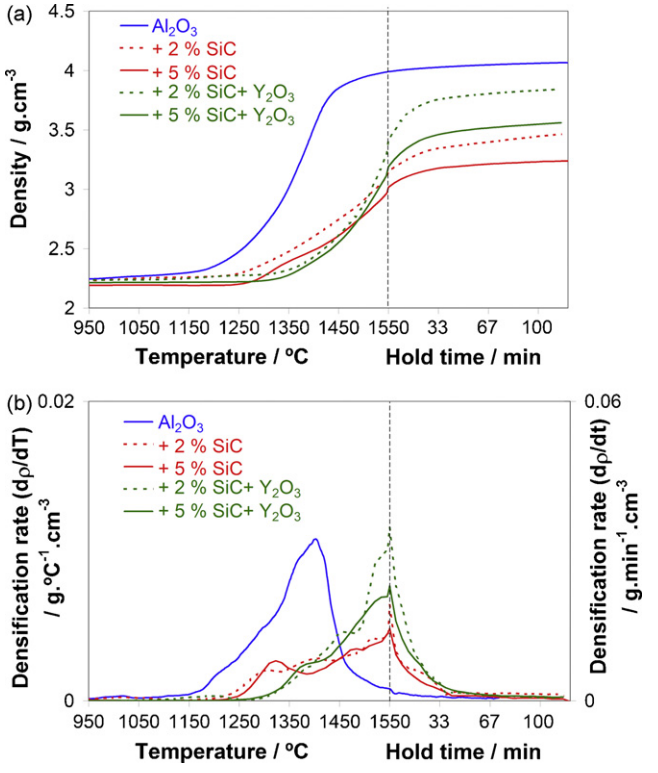


Fig. 3. Density during heating to 1550 °C and hold period (a) and differential showing rate of densification (b) for $Al_2O_3$ with and without SiC and $Y_2O_3$ additions.

The progress of sintering as monitored by dilatometry during the heating and holding phases is shown in Fig. 2a for 'pure processed' materials with and without additions of 0.1 wt.% $SiO_2$ and 0.15 wt.% $Y_2O_3$. The rate of sintering (differential of Fig. 2a with respect to time) is shown in Fig. 2b. Similarly the sintering progress for materials with and without 2 vol.% and 5 vol.% SiC and 0.15 wt.% $Y_2O_3$ are shown in Fig. 3a and b.

The addition of $Y_2O_3$ delayed the onset of sintering by ~120 °C; however, the maximum rate of densification (Fig. 2b) reached a higher value than for $Al_2O_3$ alone and eventually a high sintered density was achieved (Fig. 2a). The addition of $SiO_2$ with and without $Y_2O_3$ also delayed the onset of sintering by around 120 °C and 30 °C, respectively.

The addition of either 2 vol.% or 5 vol.% SiC delayed the onset of sintering by ~60 °C (Fig. 3b). The maximum rate of sintering was also dramatically reduced (Fig. 3b); however, the rate of sintering was reduced less with the smaller amount of SiC, which also resulted in a slightly higher sintered density (Fig. 3a). When SiC and $Y_2O_3$ were simultaneously added the onset of sintering was delayed further, by around 120 °C compared to $Al_2O_3$, for both 2 vol.% and 5 vol.% SiC; however, the rate of sintering above ~1400 °C was greater than that of the materials without $Y_2O_3$ added for both 2 vol.% and 5 vol.% SiC so that a significantly higher final density was attained. Again the material with 2 vol.% SiC had slightly higher sintering rate than that with 5 vol.% added and hence achieved a higher sintered density.

The dilatometry measurements over the temperature ranges in which densification occurred and the maximum rates are consistent with the differences in final sintered density between the materials.

### 3.2. Microstructure

A significant reduction in grain size was caused by $Y_2O_3$ addition for materials sintered at the same temperature (Table 1). The addition of SiC was also found to significantly reduce grain size compared to that of $Al_2O_3$ despite the higher sintering temperature, although there was no significant further effect when $Y_2O_3$ was also added. The $SiO_2$ addition did not increase average grain size although it caused abnormal grain growth, in particular when $Y_2O_3$ was simultaneously added.

TEM images of the 'pure' materials are shown in Figs. 4 and 5 and those of 'standard processing' materials are shown in Fig. 6. Similar trends in grain size are apparent for both groups of materials and are consistent with values measured using SEM.

Particles were found in both inter- and intra-granular locations in all of the materials although the majority of the grain boundary sections in the thin TEM specimens were without particles. The particle compositions were analysed by STEM-EDX and found to be consistent with the additions made to each material. The compositions are summarised in Table 2. Si-containing particles were found when SiC and $SiO_2$ additions were made. Although the relative carbide or oxide state of these particles could not be determined with certainty by EDX they were thought to exist in the same phase as that added. For example, Fig. 7 shows an EDX spectrum from a Si-containing particle in the 'pure' material with both SiC and

Table 1
Grain size of pure materials. (CIP in the sintering temperature column indicates that this sample was cold isostatically pressed rather than uniaxially pressed).

| Material | | | | Grain size (μm) | | | |
|---|---|---|---|---|---|---|---|
| Additions | | | Sintering temperature (°C) | Micrograph | | | **Mean** |
| SiC (vol.%) | $SiO_2$ (wt.%) | $Y_2O_3$ (wt.%) | | 1 | 2 | 3 | |
| 0 | 0 | 0 | 1550 | 3.4 | 3.3 | 2.9 | **3.2** |
| 0 | 0 | 0.15 | 1550 | 2.2 | 2.3 | – | **2.3** |
| 5 | 0 | 0 | 1775 | 2.3 | 2.5 | 2.4 | **2.4** |
| 5 | 0 | 0 | $1775^{CIP}$ | 1.8 | 2.0 | 2.0 | **1.9** |
| 5 | 0 | 0.15 | 1750 | 2.0 | 2.1 | – | **2.0** |
| 0 | 0.1 | 0 | 1550 | 2.6 | – | – | **2.6** |
| 0 | 0.1 | 0.15 | 1550 | 3.0 | – | – | **3.0** |

Bold mean values represent primary importance rather than the individual values which are of secondary importance.

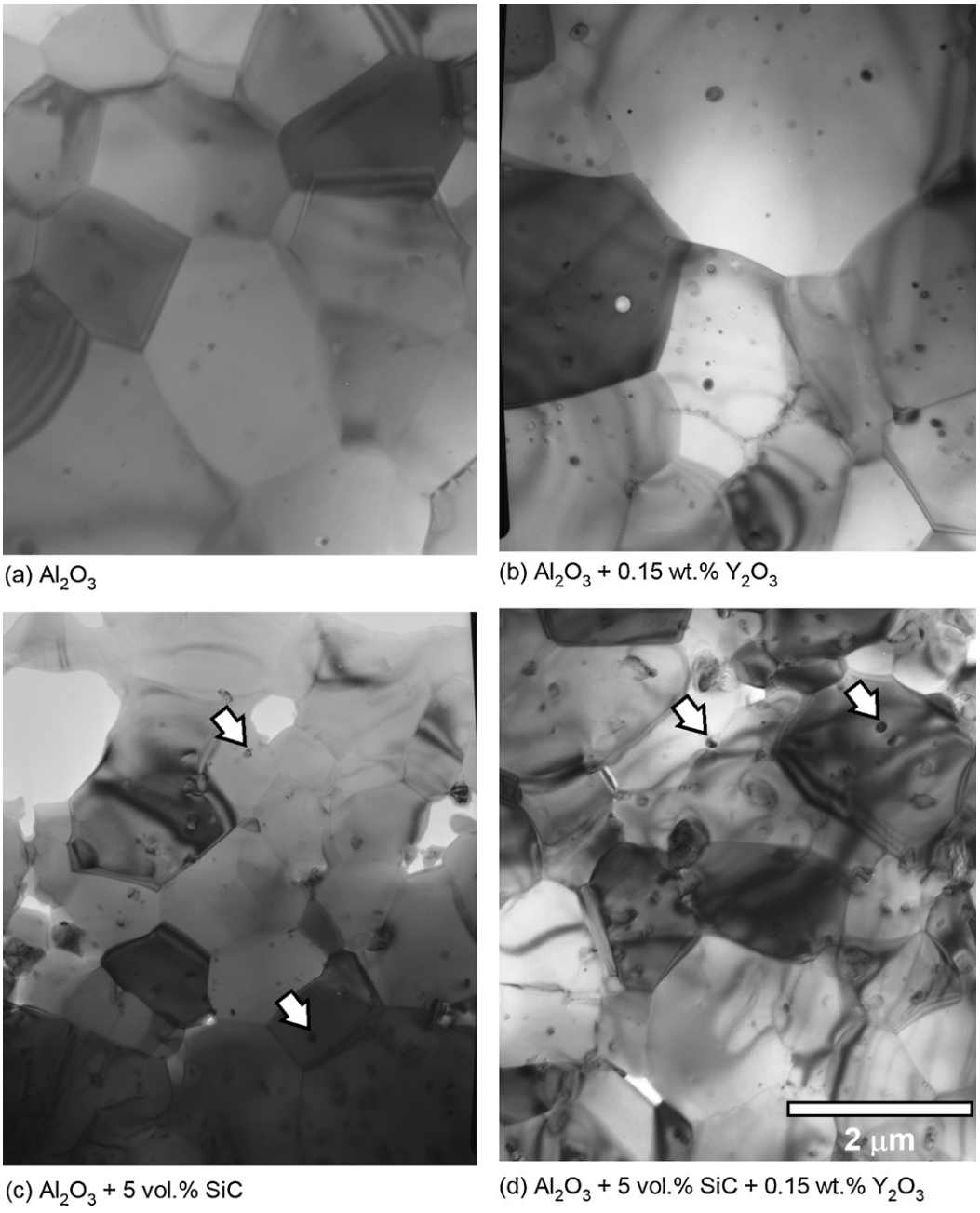


Fig. 4. Bright field TEM images of 'pure' processed materials all at the same scale. Particles are visible in all the materials, examples are indicated by arrows.

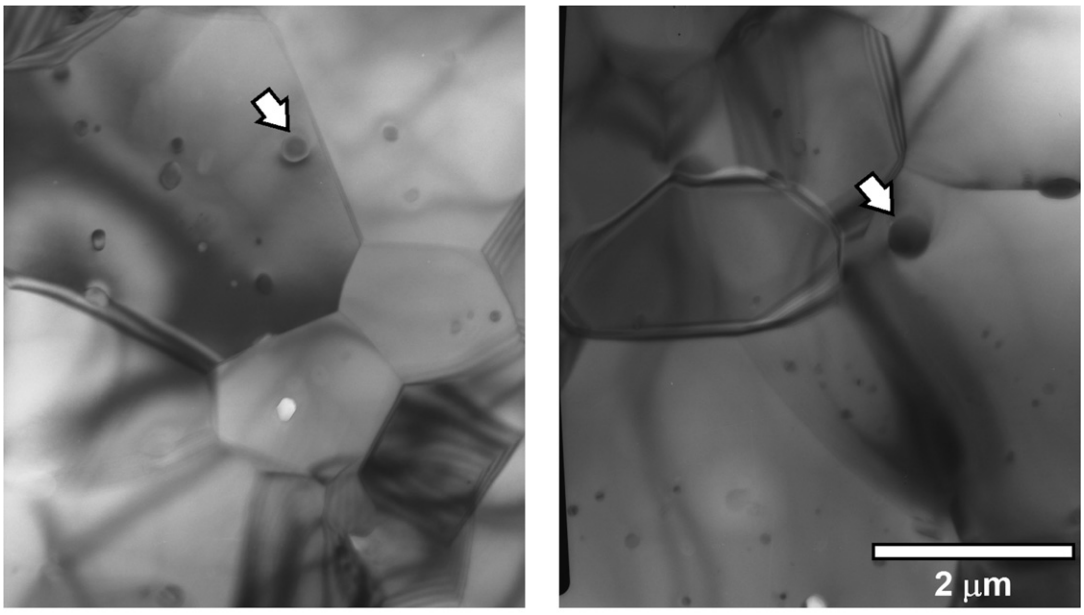


Fig. 5. 'Pure' materials with $SiO_2$ and/or $Y_2O_3$ addition. Arrows indicate examples of particles.

$Y_2O_3$ added. The small O Kα peak and large C Kα peak suggest that this is a SiC particle, with a small contribution from the $Al_2O_3$ matrix. Y-containing particles were also found in materials with $Y_2O_3$ and these sometimes also contained Si in materials with SiC or $SiO_2$ added. N-containing particles were also found in most of the materials; these are likely to result from the $N_2$ sintering atmosphere used. Zr-containing particles were found in all the 'standard processing' materials, and are likely to result from wear of the Y-stabilized $ZrO_2$ milling media.

### 3.3. Grain boundary composition

Grain boundary composition was analysed by STEM-EDX for all 'pure' and 'standard processing' materials. Fig. 8 shows EDX spectra taken on and away from a grain boundary, for the 'pure processed' material with both SiC and $Y_2O_3$ added, revealing Si and Y segregation. Fig. 8 also shows a profile of quantified Si and Y concentrations from spectra taken at points across the same grain boundary. The elements found to be segregated to grain boundaries in the 'pure' materials were largely as expected from the additions made: Si-segregation when either SiC or $SiO_2$ was added and Y-segregation when $Y_2O_3$ was added. The 'standard' materials also had additional segregation of Si and Ca which is attributed to impurities in the $Al_2O_3$ used and Zr and Y segregations which are attributed to contamination from the milling media used. This contamination obscured the effect of the additions but the general pattern of segregation was found to be the same as that in the 'pure' materials.

The average values of these monolayer segregations are shown in Table 3. In all cases the segregation of each element was less than 10% of a monolayer except for the materials with SiC and $Y_2O_3$ simultaneously added which showed significantly increased segregation of both Si and Y, up to 19.9% Si and 19.6% Y in the 'pure' material, and up to 17.2% Si and 9.0% Y in the 'standard' material.

Table 2
Summary of particles found. A tick indicates that one or more particles containing that element (exclusively or not) were found.

| | | Particles containing: | | | | | | | | |
|---|---|---|---|---|---|---|---|---|---|---|
| | Additions | Si | Y | Si + Y | N | Zr | Zr + Y | Mg | Ca | Ti |
| Standard | – | | | | | √ | √ | | | |
| | $Y_2O_3$ | | | | | √ | √ | √ | | |
| | SiC | √ | | | √ | √ | | √ | | |
| | SiC + $Y_2O_3$ | √ | | √ | √ | √ | | | √ | √ |
| Pure | – | | | | √ | | | | | |
| | $Y_2O_3$ | | √ | | √ | | | | | |
| | SiC | √ | | | √ | | | | | |
| | SiC + $Y_2O_3$ | √ | | | √ | | | | | |
| | $SiO_2$ | √ | | | √ | | | | | |
| | $SiO_2$ + $Y_2O_3$ | √ | | √ | | | | | | |

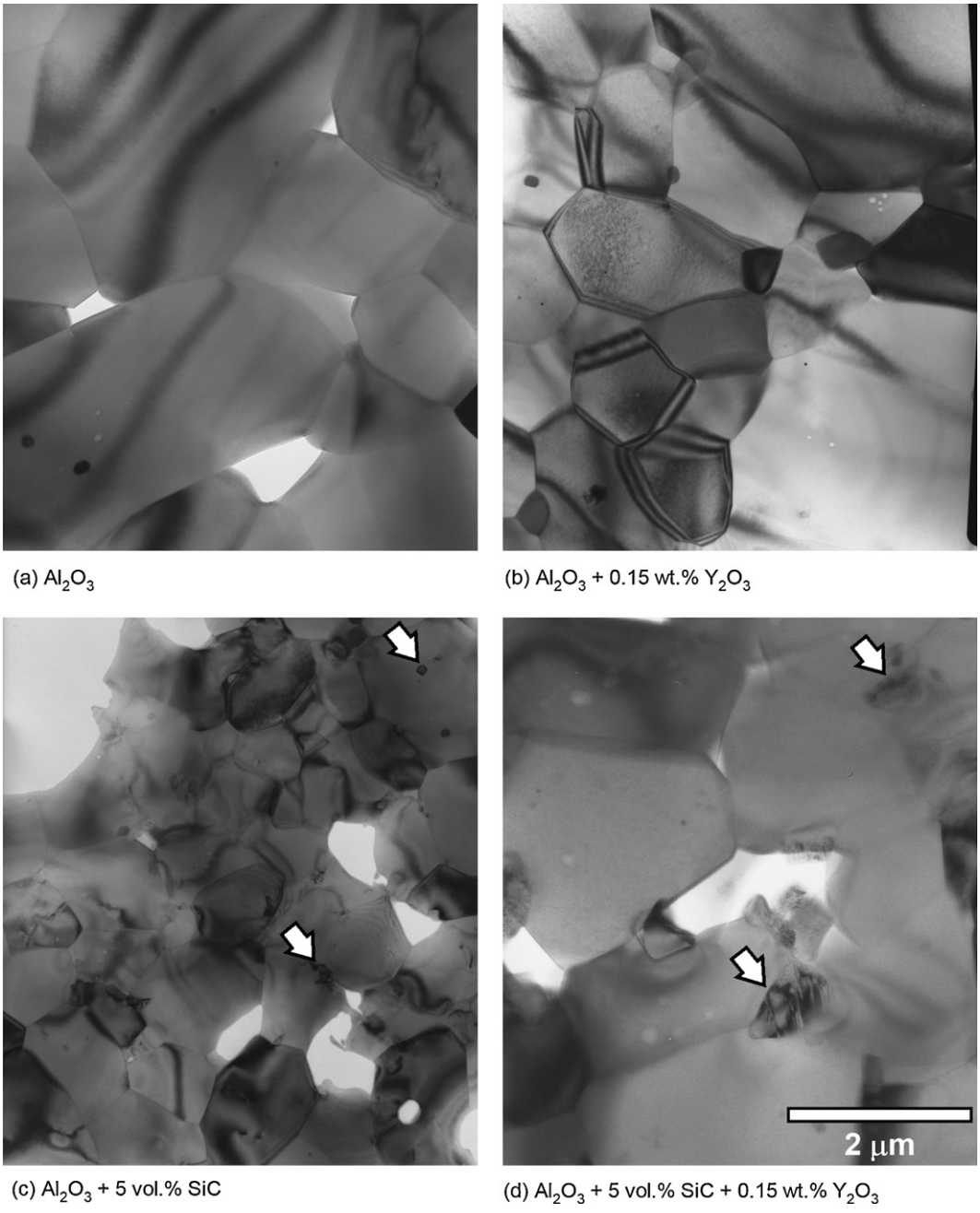


Fig. 6. Bright field TEM pictures all at the same scale of 'standard processing' materials using low purity alumina. Particles are apparent in all the materials: some examples are indicated by arrows. Grain size is obviously smaller with just SiC added (c). Some small grains and two larger grains are visible when just $Y_2O_3$ is added (b).

## 4. Discussion

### *4.1. Alumina*

#### *4.1.1. The effect of $Y_2O_3$ addition*

Grain boundary segregation in $Al_2O_3$ has an important effect on the rate of sintering and grain growth. In this work $Y_2O_3$ addition was found to delay the onset of sintering, although the maximum sintering rate (at a higher temperature) was increased compared to that in $Al_2O_3$ alone. $Y_2O_3$ addition has previously been found to reduce the sintering rate.[40,41] Sato and Carry[40] describe a regime where initially densification was hindered by a sub-saturated layer of Y-segregation at the grain boundaries (a complexion I boundary), but that as grain growth occurred grain boundaries became super-saturated (complexion III–VI) and densification was enhanced until 1500 °C, above which they observed a sudden drop in densification rate which they attributed to precipitation at the grain boundaries. Fig. 2b also shows a delay to the start of sintering, though sintering does proceed at higher temperatures. When sintering does occur, either enhanced by Sato and Carry's mechanism or simply due to higher temperature, it proceeds over a narrower temperature range than in $Al_2O_3$ perhaps due to reduced grain growth with $Y_2O_3$ present (Table 1).

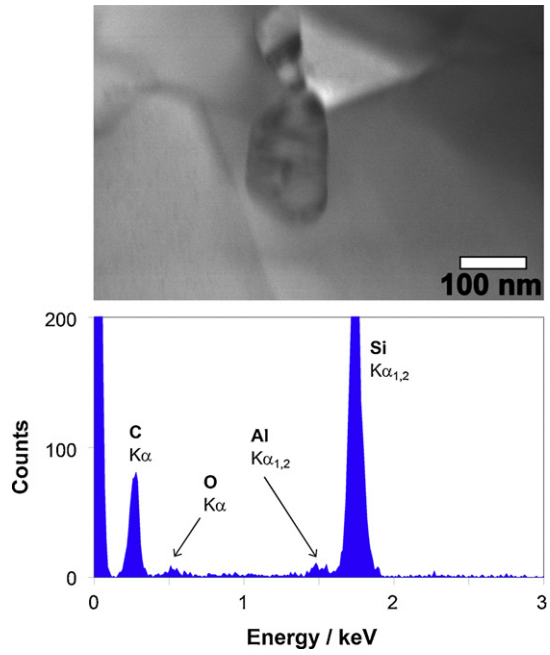


Fig. 7. BF image and EDX spectra of a Si-containing particle in 'pure' material containing SiC and $Y_2O_3$.

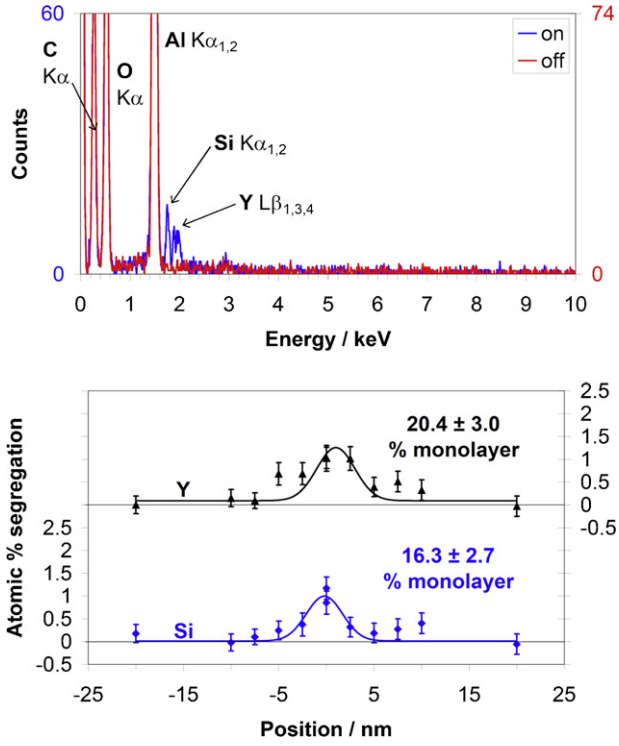


Fig. 8. EDX spectra taken on and 20 nm away from a typical grain boundary and a typical profile in 'pure' processed material with 5 vol.% SiC and 0.15 wt.% $Y_2O_3$ added.

The way in which Y-segregation affects grain boundary diffusivity has also been considered with respect to creep. Cho et al.[42] suggest that large Y-ions block diffusion. However, more recent work by Yoshida et al.[43] found that creep rate was not determined by ionic radius of various rare earth dopants and suggested that bond strength at the grain boundaries was most important. This is supported by ab initio modelling of sub-saturated (complexion I) $Al_2O_3$ grain boundaries by Buban et al.[44] which predicts that Y-segregation increases bond strength. An increased grain boundary fracture energy has been measured in $Al_2O_3$ doped with $Y_2O_3$ compared to that without, although the increase was not sufficient to cause a change to transgranular fracture.[45] This material had smaller grain size than the pure-$Al_2O_3$ and no glassy grain boundary film which suggests the grain boundaries were mainly complexion I.

$Y_2O_3$ addition to $Al_2O_3$ also caused a reduction in grain size in this work which is consistent with previous findings that $Y_2O_3$ reduces grain growth rate in $Al_2O_3$.[41] This reduction can be considered to be due to the formation of low-mobility sub-saturated, complexion I, grain boundaries.

### 4.1.2. The effect of $SiO_2$ addition

$SiO_2$ addition to $Al_2O_3$ delayed the onset of densification. $SiO_2$ addition has also previously been found to slow down sintering rate.[46] Louet et al.[46] observed that the grain boundaries were without a glassy film and suggested that Si segregation to grain boundaries would slow down diffusion mechanisms above 1200 °C due to a decrease of oxygen point defects. However, Yoshida et al.[43] who found that Si doping slowed down creep in $Al_2O_3$, predicted an increase in bond strength at the

Table 3
Average values of monolayer segregation to $Al_2O_3$–$Al_2O_3$ grain boundaries for both 'pure' and 'standard' materials.

| Processing | Additions | Number of boundaries profiled | Segregation/% of a monolayer, **average** ± standard deviation, min – max | | | |
|---|---|---|---|---|---|---|
| | | | Si | Y | Ca | Zr |
| Pure | – | 0 | **0** | **0** | **0** | **0** |
| | $Y_2O_3$ | 6 | **0** | **9.0** ± 3.5, 4.2 – 12.5 | **0** | **0** |
| | SiC | 2 | **2.6** ± 4.9, 0 – 12.1 | **0** | **0** | **0** |
| | SiC + $Y_2O_3$ | 6 | **19.9** ± 2.6, 16.3 – 23.3 | **19.6** ± 6.6, 11.1 – 29.0 | **0** | **0** |
| | $SiO_2$ | 6 | **4.3** ± 1.7, 2.7 – 7.5 | **0** | **0** | **0** |
| | $SiO_2$ + $Y_2O_3$ | 4 | **2.5** ± 1.6, 0.3 – 4.1 | **3.2** ± 0.4, 2.8 – 3.6 | **0** | **0** |
| Standard | – | 10 | **1.7** ± 2.1, 0 – 6.6 | **0** | **2.1** ± 1.2, 0.8 – 4.8 | **3.0** ± 1.8 |
| | $Y_2O_3$ | 5 | **7.5** ± 4.7, 2.7 – 12.0 | **3.4** ± 2.8, 0.2 – 6.6 | **6.4** ± 2.1, 4.0 – 8.9 | **3.0** ± 3.1, 0.1 – 7.3 |
| | SiC | 6 | **9.3** ± 1.7, 6.8 – 11.0 | **4.8** ± 1.8, 0.8 – 12.0 | **3.2** ± 1.5, 0.9 – 4.5 | **2.3** ± 1.7, 0.3 – 5.2 |
| | SiC + $Y_2O_3$ | 5 | **17.2** ± 9.5, 4.4 – 27.3 | **9.0** ± 6.4, 3.1 – 16.8 | **4.3** ± 2.1, 1.3 – 7.3 | **1.7** ± 2.4, 3.6 – 5.1 |

Bold values represents standard deviations and ranges which are of secondary importance.

glass-free grain boundaries in the presence of Si. The current study has shown a segregation of 4.3% of a monolayer when 0.1 wt.% $SiO_2$ was added which would allow either or both of these mechanisms to act.

Si segregation to $Al_2O_3$ grain boundaries has often been linked to abnormal grain growth. Bae and Baik suggested that there was a critical concentration of Si at grain boundaries, expressed as a grain boundary width, above which abnormal grain growth would occur, which depends on grain size.[47] The 'complexions' analysis would relate this width to grain boundary structure. Assuming all $SiO_2$ added contributes to grain boundary segregation, as Bae and Baik[47] did, then the 'pure' material with 0.1 wt.% $SiO_2$ added gives a grain boundary width of 3.4 nm compared to Bae and Baik's critical value of 3.7 nm. This is consistent with the observation of abnormal grain growth around the edges, where Si from the furnace elements can diffuse into the sample,[48] but not in the middle of this sample. Bae and Baik[47] did not measure the segregation in their materials, however, the 4% of a monolayer segregation measured in this work suggests that most of the $SiO_2$ addition existed as particles rather than grain boundary segregation.

A greater degree of abnormal grain growth was observed in the material with $SiO_2$ and $Y_2O_3$ simultaneously added, which had 2.5% of a monolayer Si and 3.2% of a monolayer Y segregated to the grain boundaries. This is consistent with MacLaren et al.'s[48] finding that $SiO_2$ and $Y_2O_3$ act in synergy to cause abnormal grain growth. They hypothesised that thin (<1 nm) disordered grain boundary layers, identified by HREM, were sufficient to trigger abnormal grain growth. These boundaries would be described as type IV in the 'complexions' model. They attributed the disordered grain boundaries to the segregation of Si and Y. The low levels of monolayer segregation measured in this work are consistent with such a narrow grain boundary.

The synergistic effect of Si and Y may explain why abnormal grain growth was not observed in the 'pure' processed material with $Y_2O_3$ (in which no Si segregation was measured) added but was observed[33] in the 'standard' material with $Y_2O_3$ added (in which 3.4% of a monolayer Si segregation was measured).

Comparing the measured levels of segregation with the amount of additions made indicate that some of each addition exists away from grain boundaries. As the solubility of Si[49] and Y[50] are low (<0.06 wt.%) these elements must be present either in particles (as observed) or at triple junctions. For example, if all of the 0.15 wt.% $Y_2O_3$ addition existed as grain boundary segregation between 44% and 154% of a monolayer would be expected the materials studied here (grain sizes between 1.27 μm and 4.46 μm).

### 4.2. Nanocomposites

#### 4.2.1. The effect of additions on processing

The reduction in final density and rate of sintering due to the SiC addition are consistent with each other and previous work which has described how these particles inhibit diffusion and consequently densification.[28] This work has found an increased segregation of Si to $Al_2O_3$ grain boundaries when SiC particles were added which may additionally inhibit densification in the same way that $SiO_2$ addition to $Al_2O_3$ does.

The most dramatic effect however, was the increase in maximum rate of sintering and final density when $Y_2O_3$ was added to the $Al_2O_3$/SiC nanocomposite. When compared to a nanocomposite without $Y_2O_3$ the rate of sintering at 1550 °C was increased; similarly the density after sintering at 1750 °C was increased to full density from 98.3% of theoretical density without $Y_2O_3$.

Improvement in sintering of $Al_2O_3$/SiC nanocomposites when $Y_2O_3$ is added has been previously observed.[31–33] Cock et al.[33] suggested that a glassy phase formed between $SiO_2$, $Al_2O_3$ and $Y_2O_3$[51] is responsible for the improved sintering when $Y_2O_3$ is added to $Al_2O_3$/SiC composites. The lowest temperature eutectic between these compounds melts at 1371 °C,[35] which is close to the temperature at which the $Y_2O_3$ addition suddenly became effective as a sintering aid by dilatometry in this work. Indeed below this temperature $Y_2O_3$ inhibited sintering of the nanocomposite as it did in $Al_2O_3$ without SiC addition. This work also shows that there is significant segregation, up to 20% of a monolayer each, of Si and Y to the grain boundaries when $Y_2O_3$ is added to nanocomposites. Whether this causes a glassy grain boundary layer (complexion V or VI) or the segregation simply forms a boundary with a high diffusivity grain boundary layer (complexion III or IV) would require detailed HREM analysis.

The much increased segregation in this material is presumably related to some interaction between SiC and $Y_2O_3$. Such an interaction has previously been reported by Ding et al.[52] during the sintering of SiC. They found a much greater rate of oxidation of SiC in the presence of $Y_2O_3$ and $Al_2O_3$ than they did when just $Al_2O_3$ was present. They associated this with the lower eutectic temperature of $SiO_2$–$Al_2O_3$–$Y_2O_3$ glass compared to $SiO_2$–$Al_2O_3$ glass.[35] The greater oxidation of SiC will release more $SiO_2$ which can contribute to the grain boundary glass or segregated layer, either of which may allow faster grain boundary diffusion.

#### 4.2.2. The effect of additions on $Al_2O_3$–SiC phase boundaries

The segregation to $Al_2O_3$–SiC phase boundaries was not fully studied. The curved nature of the interface through the TEM sample, together with possible thickness and X-ray count rate variations between the phases would invalidate quantification of the grain boundary composition. Detection sensitivity will also be reduced if the boundary cannot be aligned with the electron beam.

Stearns et al.'s[28] description of how SiC particles inhibit densification in $Al_2O_3$ suggests that the $Al_2O_3$–SiC interface is critical. The phase boundary composition may be expected to be related to the grain boundary composition and a $SiO_2$–$Al_2O_3$–$Y_2O_3$ eutectic phase or segregated layer may also be supposed to enhance diffusion at the phase boundary and thereby increase densification.

*4.2.3. The effect of additions on grain growth*

SiC effectively prevents grain growth, reducing the grain size of the 'pure' $Al_2O_3$ despite a raised sintering temperature. The effect has been attributed to the Zener pinning of grain boundaries by SiC particles.[28] The addition of $Y_2O_3$ to the 'pure' nanocomposite did not cause any great change in grain size, which is contrary to the abnormal grain growth found by Jeong et al. when they added 0.1 wt.% $Y_2O_3$ to a nanocomposite.[31] However, Jeong et al. sintered the material at 1800 °C for 2 h followed by hot isostatic pressing at 1600 °C which gives considerably more scope for grain growth than the 2 h sintering at 1750 °C used in this work. Abnormal grain growth was also observed when $Y_2O_3$ was added to a nanocomposite by Pillai et al.[32] but this materials also contained 0.1 wt.% $SiO_2$ impurity. Cock et al.[33] also measured a larger average grain size in the 'standard' materials (0.04 wt.% $SiO_2$ impurity) with $Y_2O_3$ added, both with and without SiC, which is consistent with the images in Fig. 6.

It seems that abnormal grain growth is most likely to occur when $Y_2O_3$ and $SiO_2$ are present together, but can be sufficiently restrained by SiC particles for some sintering schedules.

## 5. Conclusions

For the first time grain boundary segregation has been quantified in both 'pure' and less-pure 'standard' processed $Al_2O_3$ and nanocomposites, with and without $Y_2O_3$ sintering aid. The SiC addition in nanocomposites was found to increase Si segregation in both 'pure' and 'standard' processed materials. The pattern of segregation was less clear in the 'standard processing' materials due to segregation of Si, Y, Ca and Zr impurities; however, the overall pattern was thought to be the same as in the 'pure' materials; the literature reports a clear 'nanocomposite effect' for materials similar to both the 'pure' and 'standard' processed materials studied in this work.

The individual effects of Si and Y segregation and SiC particles are to hinder densification. However, the addition of $Y_2O_3$ to nanocomposites was beneficial to densification and caused increased Si and Y segregation compared to $Al_2O_3$ with only one of SiC or $Y_2O_3$ added. It is proposed that the increased segregation is due to $Y_2O_3$ promoting a reaction with SiC to form a thin $SiO_2$–$Y_2O_3$–$Al_2O_3$ glassy phase or segregated layer which increases grain and/or phase boundary diffusivity thereby improving sintering.

$Y_2O_3$ generally increases propensity for abnormal grain growth in $Al_2O_3$, particularly in the presence of $SiO_2$. However, grain growth was sufficiently restrained by SiC particles for abnormal grain growth to be absent in the nanocomposites studied here.

## Acknowledgement

This research was supported by the Engineering and Physical Sciences Research Council (UK), under grant N06601.

## References

1. Niihara, K. and Nakahira, A., In '*Advanced Structure Inorganic Composites*' ed. P. Vincenzini. Elsevier Science Publishers, London, 1991, p. 637.
2. Zhao, J., Stearns, L. C., Harmer, M. P., Chan, H. M. and Miller, G. A., Mechanical behaviour of alumina–silicon carbide "Nanocomposites". *J. Am. Ceram. Soc.*, 1993, **76**, 503–510.
3. Davidge, R. W., Brook, R. J., Cambier, F., Poorteman, M., Leriche, A., O'Sullivan, D., Hampshire, S. and Kennedy, T., Fabrication, properties and modelling of engineering ceramics reinforced with nanoparticles of silicon carbide. *Br. Ceram. T*, 1997, **96**, 121–127.
4. Borsa, C. E., Jiao, S., Todd, R. I. and Brook, R. J., Processing and properties of $Al_2O_3$/SiC nanocomposites. *J. Microsc.*, 1995, **177**, 305–312.
5. Carroll, L., Sternitzke, M. and Derby, B., Silicon carbide particle size effects in alumina-based nanocomposites. *Acta Mater.*, 1996, **44**, 4543–4552.
6. Perez-Rigueiro, J., Pastor, J. Y., Llorca, J., Elices, M., Miranzo, P. and Moya, J. S., Revisiting the mechanical behavior of alumina silicon carbide nanocomposites. *Acta Mater.*, 1998, **46**, 5399–5411.
7. Tan, H. and Yang, W., Toughening mechanisms of nanocomposite ceramics. *Mech. Mater.*, 1998, **30**, 111–123.
8. Walker, C. N., Borsa, C. E., Todd, R. I. and Brook, R. J., Fabrication, processing and properties of alumina matrix nanocomposites. *Br. Ceram. Soc.*, 1994, **53**, 249–264.
9. Kara, H. and Roberts, S. G., Polishing behaviour and surface quality of alumina and alumina/silicon carbide nanocomposites. *J. Am. Ceram. Soc.*, 2000, **83**, 1219–1225.
10. Wu, H. Z., Surface damage and strengthening in alumina/silicon carbide nanocomposites. *D. Phil. Thesis*, Oxford University, U.K., 2001.
11. Wu, H. Z., Roberts, S. G. and Derby, B., Microstructure and residual stress of machined $Al_2O_3$/SiC nanocomposite surfaces. *Acta Mater.*, 2001, **49**, 507–517.
12. Tanner, B. K., Wu, H. Z. and Roberts, S. G., Sub-surface damage in ground and annealed alumina and alumina–silicon carbide nanocomposites. *J. Am. Ceram. Soc.*, 2006, **89**, 3745–3750.
13. Wu, H. Z., Roberts, S. G. and Derby, B., Fluorescence probe residual stress measurements around indentations and scratches in alumina and alumina/SiC nanocomposites. *Acta Mater.*, 2008, **56**, 140–149.
14. Ortiz-Merino, J. L. and Todd, R. I., Relationship between wear rate, surface pullout and microstructure during abrasive wear of alumina and alumina/SiC nanocomposites. *Acta Mater.*, 2005, **53**, 3345–3357.
15. Wu, H. Z., Roberts, S. G., Möbus, G. and Inkson, B. J., Subsurface damage analysis by TEM and 3D FIB crack mapping in alumina and alumina/5vol%SiC nanocomposites. *Acta Mater.*, 2003, **51**, 149–163.
16. Baron, B., Kumar, C. S., Le Gonidec, G. and Hampshire, S., Comparison of different alumina powders for the aqueous processing and pressureless sintering of $Al_2O_3$–SiC nanocomposites. *J. Eur. Ceram. Soc.*, 2002, **22**, 1543–1552.
17. Sciti, D., Vicens, J. and Bellosi, A., Microstructure and properties of alumina–SiC nanocomposites prepared from ultrafine powders. *J. Mater. Sci.*, 2002, **37**, 3747–3758.
18. Kara, H. and Roberts, S. G., Wet erosion behaviour of low SiC alumina–SiC nanocomposites. *J. Mater. Sci.*, 2002, **37**, 2421–2426.
19. Ohji, T., Hirano, T., Nakahira, A. and Niihara, K., Particle/matrix interface and its role in creep inhibition in alumina/silicon carbide nanocomposites. *J. Am. Ceram. Soc.*, 1996, **79**, 33–45.
20. Jiao, S., Jenkins, M. L. and Davidge, R. W., Interfacial fracture energy–mechanical behaviour relationships in $Al_2O_3$/SiC and $Al_2O_3$/TiN nanocomposites. *Acta Mater.*, 1997, **45**, 149–156.
21. Ferroni, L. P., Pezzotti, G., Isshiki, T. and Kleebe, H.-J., Determination of amorphous interphacial phases in $Al_2O_3$/SiC nanocomposites by computer-aided high-resolution electron microscopy. *Acta Mater.*, 2001, **49**, 2109–2113.
22. Levin, I., Kaplan, W. D., Brandon, D. G. and Wieder, T., Residual stresses in alumina–SiC nanocomposites. *Acta Metall. Mater.*, 1994, **42**, 1147–1154.
23. Todd, R. I., Bourke, M. A. M., Borsa, C. E. and Brook, R. J., Neutron diffraction measurements of residual stresses in alumina/SiC nanocomposites. *Acta Mater.*, 1997, **45**, 1791–1800.

24. Dillon, S. J. and Harmer, M. P., Demystifying the role of sintering additives with "complexion". *J. Eur. Ceram. Soc.*, 2008, **28**, 1485–1493.
25. Dillon, S. J., Tang, M., Carter, W. C. and Harmer, M. P., Complexion: a new concept for kinetic engineering in materials science. *Acta Mater.*, 2007, **55**, 6208–6218.
26. Schmid, H. K., Aslan, M., Assmann, S., Naß, R. and Schmidt, H., Microstructural characterization of $Al_2O_3$–SiC nanocomposites. *J. Eur. Ceram. Soc.*, 1998, **18**, 39–49.
27. Deng, Z.-Y., Zhou, Y., Brito, M. E., Tanaka, Y. and Ohji, T., Effects of rare earth dopants on grain boundary bonding in alumina–silicon carbide composites. *J. Eur. Ceram. Soc.*, 2004, **24**, 511–516.
28. Stearns, L. C., Zhao, J. and Harmer, M. P., Processing and microstructure development in $Al_2O_3$–SiC "nanocomposites". *J. Eur. Ceram. Soc.*, 1992, **10**, 473–477.
29. Anya, C. C. and Roberts, S. G., Pressureless sintering and elastic constants of $Al_2O_3$/SiC nanocomposites. *J. Eur. Ceram. Soc.*, 1997, **17**, 565–573.
30. Wang, J., Lim, S. Y., Ng, S. C., Chew, C. H. and Gan, L. M., Dramatic effect of a small amount of MgO addition on the sintering of $Al_2O_3$–5 vol% SiC nanocomposite. *Mater. Lett.*, 1998, **33**, 273–277.
31. Jeong, Y.-K., Nakahira, A. and Niihara, K., Effects of additives on microstructure and properties of alumina–silicon carbide nanocomposites. *J. Am. Ceram. Soc.*, 1999, **82**, 3609–3612.
32. Pillai, S. K. C., Baron, B., Pomeroy, M. J. and Hampshire, S., Effect of oxide dopants on densification, microstructure and mechanical properties of alumina–silicon carbide nanocomposite ceramics prepared by pressureless sintering. *J. Eur. Ceram. Soc.*, 2004, **24**, 3317–3326.
33. Cock, A. M., Shapiro, I. P., Todd, R. I. and Roberts, S. G., Effects of yttrium on the sintering and microstructure of alumina–silicon carbide "nanocomposites". *J. Am. Ceram. Soc.*, 2005, **88**, 2354–2361.
34. Noguchi, T. and Mizuno, M., Kogyo Kogaku Zasshi, 1967, **70**, 839 as reproduced in Figure 4370 of Levin, E. M. and McMurdie, H. F., *Phase Diagrams for Ceramists, 1975 Supplement'*, ed. Reser M. K., American Ceramic Society, USA, 1975.
35. Kolitsch, U., Seifert, H. J., Ludwig, T. and Aldinger, F., Phase equilibria and crystal chemistry in the $Y_2O_3$–$Al_2O_3$–$SiO_2$ system. *J. Mater. Res.*, 1999, **14**, 447–455.
36. Smith, C. S. and Guttman, L., Measurement of internal boundaries in three-dimensional structures by random sectioning. *Trans. Am. Inst. Min. Metall. Eng.*, 1953, **197**, 81–87.
37. Mendelson, M. I., Average grain size in polycrystalline ceramics. *J. Am. Ceram. Soc.*, 1969, **52**, 443–446.
38. Vatter, I. A. and Titchmarsh, J. M., Comparison of FEG-STEM and AES measurements of equilibrium segregation of phosphorus in 9% Cr ferritic steels. *Surf. Interf. Anal.*, 1997, **25**, 760–776.
39. Vatter, I. A. and Titchmarsh, J. M., Measurement of grain-boundary segregation by STEM-EDX analysis. *Ultramicroscopy*, 1989, **28**, 236–239.
40. Sato, E. and Carry, C., Yttria doping and sintering of submicrometer-grained α-alumina. *J. Am. Ceram. Soc.*, 1996, **79**, 2156–2160.
41. Voytovych, R., MacLaren, I., Gülgün, M. A., Cannon, R. M. and Rühle, M., The effect of yttrium on densification and grain growth in α-alumina. *Acta Mater.*, 2002, **50**, 3453–3463.
42. Cho, J., Harmer, M. P., Chan, H. M., Rickman, J. M. and Thompson, A. M., Effect of yttrium and lanthanum on the tensile creep behavior of aluminum oxide. *J. Am. Ceram. Soc.*, 1997, **80**, 1013–1017.
43. Yoshida, H., Ikuhara, Y. and Sakuma, T., Grain boundary electronic structure related to the high-temperature creep resistance in polycrystalline $Al_2O_3$. *Acta Mater.*, 2002, **50**, 2955–2966.
44. Buban, J. P., Matsunaga, K., Chen, J., Shibata, N., Ching, W. Y., Yamamoto, T. and Ikuhara, Y., Grain boundary strengthening in alumina by rare earth impurities. *Science*, 2006, **311**, 212–215.
45. Takigawa, Y., Ikuhara, Y. and Sakuma, T., Grain boundary bonding state and fracture energy in small amount of oxide-doped fine-grained $Al_2O_3$. *J. Mater. Sci.*, 1999, **34**, 1991–1997.
46. Louet, N., Reveron, H. and Fantozzi, G., Sintering behaviour and microstructural evolution of ultrapure α-alumina containing low amounts of $SiO_2$. *J. Eur. Ceram. Soc.*, 2008, **28**, 205–215.
47. Bae, I.-J. and Baik, S., Abnormal grain growth of alumina. *J. Am. Ceram. Soc.*, 1997, **80**, 1149–1156.
48. MacLaren, I., Cannon, R. M., Gülgün, M. A., Voytovych, R., Popescu-Pogrion, N., Scheu, C., Täffner, U. and Rühle, M., Abnormal grain growth in alumina: synergistic effects of yttria and silica. *J. Am. Ceram. Soc.*, 2003, **86**, 650–659.
49. Lee, C. H. and Kröger, F. A., Electrical conductivity of polycrystalline $Al_2O_3$ doped with silicon. *J. Am. Ceram. Soc.*, 1985, **68**, 92–99.
50. Cawley, J. D. and Halloran, J. W., Dopant distribution in nominally yttrium-doped sapphire. *J. Am. Ceram. Soc.*, 1986, **69**, C195–C196.
51. Bonder, I. A. and Galakhov, F. Y., Phase equilibria in the system $Y_2O_3$–$Al_2O_3$–$SiO_2$. Izv. Akad. Nauk. SSSR, Ser. Kim., 1963, **7**, 1325–1326. As reproduced in Levin, E. M., Robbins, C. R. and McMurdie, H. F., *Phase Diagrams for Ceramists, 1969 Supplement'*, ed. Reser M. K., American Ceramic Society, USA, 1969.
52. Ding, S. Q., Zhu, S. M., Zeng, Y. P. and Jiang, D. L., Effect of $Y_2O_3$ addition on the properties of reaction-bonded porous SiC ceramics. *Ceram. Int.*, 2006, **32**, 461–466.